This manuscript is a preprint and has been submitted for publication in **Geophysical Research Letters**. The manuscript is currently undergoing the peer-review process. Subsequent versions of this manuscript may have slightly different content. If accepted, the final version of this manuscript will be available via the 'Peer-reviewed Publication DOI' link on the right-hand side of this webpage. Please feel free to contact any of the authors; we welcome feedback.

Fluid surface coverage showing the controls of rock mineralogy on the wetting state

Gaetano Garfi, Cédric M. John, Qingyang Lin, Steffen Berg, Samuel Krevor

[1]Imperial College London, Department of Earth Science and Engineering, London, UK
[2]Imperial College London, Department of Earth Science and Engineering, London, UK
[3]Imperial College London, Department of Earth Science and Engineering, London, UK
[4]Shell Global Solutions International B.V., Amsterdam, The Netherlands and Imperial College London, Department of Earth Sciences and Engineering, Department of Chemical Engineering, London, UK
[5]Imperial College London, Department of Earth Science and Engineering, London, UK

Key Points:

- The analysis of fluid surface coverage is proposed as a novel approach to rock wettability characterisation
- A thermodynamically constrained model is derived and test on a Bentheimer sandstone water-wet X-ray micro-CT dataset
- In a Berea sandstone, fluid surface coverage shows that rock mineralogy controls system local wettability after exposure to crude oil

Corresponding author: Gaetano Garfi, `g.garfi17@imperial.ac.uk`

Abstract

The wetting state is an important control on flow in subsurface multi fluid phase systems, e.g., carbon storage and oil production. Advances in X-ray imaging allow us to characterise the wetting state using imagery of fluid arrangement within the pores of rocks. We derived a model from equilibrium thermodynamics relating fluid coverage of rock surfaces to wettability and fluid saturation. The model reproduces the behaviour measured in a water-wet, nearly all-quartz, Bentheimer sandstone imaged during steady-state imbibition. A shift in fluid surface coverage is observed when the rock is altered to a new wetting state with crude oil. In two multi-mineralogical (Berea) samples, one water-wet and the other altered with crude oil, the analysis of fluid surface coverage after imbibition revealed mineral specific wetting preferences only in the altered system. Clays and calcite preferentially alter to an oil wet state, leading to mixed wettability in the rock.

Plain Language Summary

When contacted by two or more fluids a solid surface may exhibit a preference for being coated by one of these fluids. This preference, called wetting preference, is crucial in defining how the fluids move in porous rocks or any other porous media of interest. The investigation of this wetting preference, defined wettability, is complex and several possible approaches are available in literature. In this study, we propose a novel approach based on the intuitive concept that the more a surface prefers to be coated by a certain fluid, the larger will be this coating, fixed the fluids' volume into the rock pores. The viability of our approach is first proven by considering two rock samples constituted by a unique material, but possessing different wetting preference. Eventually, we make use of our approach to better understand how in rocks constituted by a number of diverse materials, these materials behave in different ways when exposed to crude oil, mimicking the processes that happen in oil reservoirs. A deeper comprehension of this behaviour could aid the design of more efficient hydrocarbon production processes.

1 Introduction

Wettability is an important control in subsurface fluid flow, where fluids move through pore networks where capillary forces are dominant (Zou et al., 2018; Rücker et al., 2019; Lin et al., 2019). During oil recovery rock wettability exerts a control on the capillary entry pressure during primary drainage or in determining the likelihood of snap-off events of the non-wetting phase during waterflooding (Blunt et al., 2002). As a consequence of pore scale fluid dynamics, the behaviours of continuum scale properties such as relative permeability and capillary pressure are controlled by the wetting state (Anderson, 1987a, 1987b).

Predicting and characterising the wettability of an oil reservoir is a complex task. Minerals constituting rocks are naturally water-wet in the absence of hydrocarbon deposits. However, many oil reservoirs show relative permeability and capillary pressure functions indicative of intermediate-wet, mixed-wet or oil-wet systems (Donaldson et al., 1969). Indeed, rock surface wetting preference may be altered by the interaction of the solid substrate with surface-active compounds present in the crude oil. If present, these compounds can precipitate or diffuse to the solid surface and be adsorbed modifying the local wetting state (J. S. Buckley & Liu, 1998; J. S. Buckley, 1998). The results of these alteration mechanisms are dependent on the thermodynamic conditions, crude oil composition, brine composition and solid surface chemistry.

A number of studies have characterised the wetting behaviour of minerals typically found in the subsurface, i.e., in carbonate and sandstone reservoirs. A summary of the results of a collection of studies can be found in J. S. Buckley (1998). Calcite and clay minerals have been found to be more responsive to wettability alteration by crude oil exposure than quartz (Alipour Tabrizy et al., 2011). However, experiments on chemically homogeneous flat surfaces or powders can only reproduce uniform altered wettability in the system considered. In order to investigate the role of rock geometrical complexity and mineralogical heterogeneity in determining the *in situ* wetting state, it is necessary to study three-dimensional samples.

X-ray micro-CT offers the opportunity to investigate fluid arrangement inside rock pores (Bultreys, Boone, et al., 2016; Bultreys, De Boever, & Cnudde, 2016; Coles et al., 1996). With this newfound capability, thermodynamic theory indicates that it should be possible to observe wetting signals from *in situ* contact angles, interfacial fluid curvature and fluid-solid surface coverage (Morrow & Szabo, 1970). *In situ* contact angles have been measured - either manually (Andrew et al., 2014; Singh et al., 2016) or automatically (Klise et al., 2016; Scanziani et al., 2017; AlRatrout et al., 2017) - in the pore space of various rock samples identifying different wetting states (Rücker et al., 2019; Alhammadi et al., 2017). However, the measurements typically obtained have shown a large variability in space and sensitivity to the processing pipeline chosen (Garfi et al., 2019), making their direct employment difficult. Mean interfacial fluid curvature has successfully been employed to map capillary pressure in water-wet and intermediate-wet rock samples (Herring et al., 2017; Garing et al., 2017; Lin, Bijeljic, Pini, et al., 2018a; Lin et al., 2019). However, the interpretation of mean interfacial curvature as a signal of wetting is not straightforward: when the system is not water-wet, interfaces tend to have null mean curvature, meaning that their curvature has opposite sign along the two principal radii of curvature (Lin et al., 2019). Eventually, fluid-solid surface coverage as a signal of wetting has not been explored thoroughly and its potential is still outstanding.

In this study, we show that the characterisation of fluid coverage of rock surfaces can depict changes in the local wetting state. We develop and validate a simple model, based in the thermodynamics of fluid-solid interfaces of a water wet system, to demonstrate the applicability of solid surface coverage as a measure of wetting. Fluid-solid interfacial areas are then measured to characterise the wetting state of two rock lithologies. We first make use of observations on a mono-mineralogical rock (Bentheimer sandstone) as a case study to test the approach. We then extend our approach to chemically heterogeneous systems and investigate mineral specific wettability in two Berea sandstone samples - one in its original state and one exposed to crude oil to alter the natural mineral wetting preference - by performing two drainage-waterflooding cycle experiments and comparing the fluid arrangement observed in the two images acquired after waterflooding.

2 Materials and Methods

2.1 Mono-mineralogical system: Bentheimer sandstone datasets

In this work we first make use of two datasets created by Lin, Bijeljic, Pini, et al. (2018a) and Lin et al. (2019) as a case study with a simplified mineralogy. Bentheimer sandstone is 98% quartz, 1% kaolinite/chlorite and 1% microcline, but for the purposes of this work it was assumed to be a homogeneous rock constituted of a single mineralogy. All the images were segmented into rock, brine and oil phases (Lin, Bijeljic, Pini, et al., 2018a; Lin et al., 2019). In our study the region of interest used in the analysis was $900 \times 900 \times 3000$ voxels with $3.58\,\mu m$ voxel side, i.e. the spatial domain analysed was $3.22 \times 3.22 \times 10.74\,\mathrm{mm}^3$.

The first dataset - that we call Bentheimer Unaltered - consisted of the X-ray micro-CT images acquired with two-fluid injection at five fractional flows ($f_w = q_w/(q_w + q_o)$ where q_i are volume flow rates of brine and oil) (S. Buckley & Leverett, 1942) of the wetting phase, brine phase ($f_w = \{0.15, 0.30, 0.50, 0.85, 1\}$), during steady-state imbibition (brine fractional flow increasing with each step). The fluids in the system were brine (3.5 wt% KI) and decalin. For further information please refer to Lin, Bijeljic, Pini, et al. (2018a).

The second dataset - that we call Bentheimer Altered - used a sample that was very similar to the Bentheimer Unaltered, except that the wetting state was altered before the coreflood. Prior to the flow experiments, this sample was partially saturated with crude oil and heated at 80°C for 30 days in a wetting alteration process known as ageing. The fluids in this case were brine (3.5 wt% KI, 1.09 wt% NaCl, 0.02 wt% $MgCl_2.6H_2O$, 0.11 wt% $CaCl_2.2H_2O$) and decalin (Lin et al., 2019; Lin, Bijeljic, Krevor, et al., 2018). Five images at fractional flow steps $f_w = \{0.24, 0.50, 0.80, 0.90, 1\}$ were considered in this study.

2.2 Multi-mineralogical system: experiments on Berea sandstone

2.2.1 Rock samples

Two Berea sandstone samples of 4 mm in diameter and 20 mm in length were drilled from the same core. This core has laminations of cemented calcite. The main mineral groups present were identified by scanning electron microscopy (SEM) operated in back scattered electron (BSE) mode and coupled with energy-dispersive X-ray spectroscopy (EDS). Quartz grains constitute the majority of the rock matrix. The other mineral groups identified were clay group minerals (kaolinite, illite and smectite), potassium feldspar and small traces of minerals embedding metals. A reference example of mineral characterisation of Berea sandstone may be found in Lai et al. (2015). As with the Bentheimer, one of the samples was used unaltered by crude oil and is referred to as Berea Unaltered. The other sample underwent crude oil exposure after primary drainage and will be referred to as Berea Altered.

2.2.2 Fluids, fluid injection strategy, and wettability alteration

Two drainage-imbibition cycle experiments were performed. In the experiment involving Berea Unaltered, the fluids employed were brine (15 wt% KI in de-ionized water) and decane. The sample was firstly saturated with brine at atmospheric pressure and then pressurized at the injection pressure of 3.5 MPa. Decane was thus injected at a flow rate of 0.015 $\frac{\text{ml}}{\text{min}}$, which corresponds to a capillary number $N_c \approx 10^{-7}$. The total injected volume of decane was 2.5 ml. The injection was stopped for at least 4 hours in addition to the scanning time, before performing brine injection. 40 pore volumes were injected at a constant flow rate of 0.015 $\frac{\text{ml}}{\text{min}}$.

In the experiment with the sample Berea Altered, the fluids employed were brine (15 wt% KI, 1.09 wt% NaCl, 0.02 wt% $MgCl_2.6H_2O$, 0.11 wt% $CaCl_2.2H_2O$) and crude oil (density $\rho = 0.8540\,\text{kg/m}^3$ and viscosity $\mu = 4.7765\,\text{mPa s}$ at 20°C). The sample was firstly saturated with brine. Crude oil drainage was then performed by setting a constant pressure gradient of 5 Mpa between the injection and the receiving pumps, up to a total volume injection of 2.5 ml. After drainage, the sample was then removed from the coreholder and stored immersed in crude oil in a sealed glass bottle. The glass bottle was put into an oven at a temperature of 80°C for 30 days. After the wettability alteration protocol, the sample was mounted in the coreholder and waterflooding was performed, by injecting 40 pore volumes of brine at a constant flow rate of 0.015 $\frac{\text{ml}}{\text{min}}$.

In both the experiments, after waterflooding the injection was stopped and the system was allowed to equilibrate for 4 hours to a pressure of 3.5 MPa.

2.2.3 Imaging and Image processing of Berea sandstone: minerals and fluids phase segmentation

The samples were imaged with an FEI Heliscan microCT obtaining a voxel resolution of 2.0 μm for a region of interest larger than the sample cross section and a vertical length of 8 mm. The projections were acquired while the sample was moving along a helical trajectory and a 1 mm thick aluminium filter was employed. The X-ray source voltage was set to 95 kV and the tube current to 70 mA. The raw images were reconstructed employing an iterative back-projection algorithms provided by the scanner manufacturer. For both samples, images were acquired before the injection of any fluid (referred to as the dry scan) and after waterflooding.

The processing steps were the same for both samples. We filtered the dry scan and waterflooding image by non-local means filtering (Buades et al., 2005) and registered them. The greyscale dry scans were segmented using watershed segmentation (Beucher & Meyer, 1993) into five phases: pore space, clay group minerals, quartz-feldspar group minerals, cemented calcite and others highly attenuating minerals. The filtered waterflooding image was masked with the segmented pore space image, leading us to the segmentation of the two fluid phases (oil phase and brine phase) by simple thresholding. The region of interest of our analysis for each image was a cube of 1200 voxel side, i.e. 2.4 mm.

2.3 Rock surface coverage as a measure of wetting: a model for water-wet systems

Consider a porous medium comprising two fluid phases, a wetting phase, w, and a non-wetting phase, o, e.g., oil, and a solid phase, s. Per unit volume of pore space, the reversible work required to increase the saturation of a non-wetting phase results in the creation of fluid-fluid interfaces, between wetting phase, non-wetting phase, and the solid (Morrow & Szabo, 1970; Bradford & Leij, 1997),

$$P_c \mathrm{d}S_o = \sigma_{ow}\mathrm{d}A_{ow} + \sigma_{os}\mathrm{d}A_{os} + \sigma_{ws}\mathrm{d}A_{ws} \tag{1}$$

P_c is the capillary pressure, S_i is the saturation with $S_o = 1 - S_w$, σ_{ij} is the interfacial tension between fluid or solid phase i and phase j, and A is the interfacial area per unit volume of pore space between phases.

The use of reversible work in the analysis is equivalent to limiting our consideration to equilibrium states of the system, i.e., $P_c(S_o)$ and $A_{ij}(S_o)$ at equilibrium. We ignore irreversible work that may be required in practice to move from one state to the next, e.g., due to transient processes (Berg et al., 2013; Morrow & Szabo, 1970). This is the assumption made when making use of capillary pressure characteristic curves as constitutive laws in the description of subsurface flow.

By integrating Eq.1, followed by algebraic operations and making use of the Laplace relationship, $P_c = 2\kappa\sigma_{ow}$, where κ is the mean interfacial curvature of the oil-brine interface, it is possible to derive the following (see the Supporting Information for a full derivation):

$$A_{os}(S_o) = \frac{1}{\beta}\frac{\sigma_{ow}}{\sigma_{os} - \sigma_{ws}}\left(2\int_{S'=0}^{S_o} \kappa \mathrm{d}S' - \int_{S'=0}^{S_o} \frac{\mathrm{d}A_{ow}}{\mathrm{d}S'}\mathrm{d}S'\right) \tag{2}$$

The terms inside the brackets represent the reversible work of desaturation and the creation of oil-water interfacial area, respectively. The equation expresses the oil-solid interfacial area created from the excess energy available when subtracting the work required for the creation of fluid-fluid interfacial area from the work performed to increase the saturation of the non-wetting phase in the rock. The multiplier term with the ratio of interfacial tensions is equivalent to $\frac{1}{\cos\theta}$ in a single capillary tube (θ is the contact angle). Without changing sign entirely, the more wetting the solid is with respect to the non-wetting phase (the smaller the value of σ_{os}), the more interfacial area between the non-wetting phase and solid, A_{os}, will be created per unit of work. The parameter β represents a roughness factor that accounts for the mismatch between the real surface area shared by each fluid and the solid surface and the one measurable by imaging, due to imaging resolution limit (Helgeson et al., 1984; White & Peterson, 1990).

2.4 Rock surface coverage characterisation by micro-CT imaging

In order to characterise rock surface coverage, the interfaces between mineral phases and fluid phases were identified. In the case of the Bentheimer datasets two groups of interfaces were identified, between oil and rock, and between brine and rock phases. In the case of the multi-mineral Berea sandstone, having produced segmented images with four mineral phases and two fluids, we identified a total of eight interface groups, i.e., for each mineral and both fluid phases. Once an interface of interest was identified, a smooth surface was constructed through that interface by means of a generalized marching cubes algorithm.

We compare fluid surface coverage of different minerals by defining the fraction of the total area of that mineral in contact with a fluid:

$$a_{i,j} = \frac{A_{i,j}}{\sum_i A_{i,j}} \tag{3}$$

where $A_{i,j}$ is the measured surface area per unit of pore volume shared by mineral i with fluid j, respectively. The fractional definition of this property serves two purposes: to allow for the comparison of the specific wetting preference of different mineral groups with different total mineral-to-pore surface areas; to make the measurement more robust to the surface smoothing and to the image processing pipeline chosen.

3 Results and Discussion

3.1 Bentheimer sandstone: fluid coverage of chemically homogeneous rock surfaces

The region of interest for the ten images considered (five for Bentheimer Unaltered and five for Bentheimer Altered) was divided into 90 cubic subvolumes of 300 voxels per side (voxel side $3.58\,\mu m$). This allowed us to obtain a more precise topological description of the wetting state of the system investigated. In each of the subvolumes, for each of the images and each of the datasets, fluid saturations, rock volume and fluid-coated interfacial areas were computed.

The results obtained from the employment of our approach to wettability characterisation reconciled well with the authors' assumptions that Bentheimer Unaltered was water-wet (Lin, Bijeljic, Pini, et al., 2018a) and Bentheimer Altered was intermediate or mixed wetting to oil (Lin et al., 2019). Specific oil-rock interfacial area measurements are reported as a function of saturation for each of the subvolumes and for each of the fractional flow considered in the two datasets Bentheimer Unaltered and Bentheimer Altered in Figure 1. For similar oil saturation values, in the intermediate-wet - Bentheimer Altered - sample rock coverage by oil is larger. As expected in a mixed or intermediate wet system, oil is more likely to coat the solid surface than in a water-wet system. Figure 1 also shows that the model we proposed for water-wet systems (Eq.2) well reproduce the behaviour of the measured specific oil-rock interfacial area datapoints in Bentheimer Unaltered dataset. By fitting the model to the experimental data, we estimated $\frac{1}{\beta}\frac{\sigma_{ow}}{\sigma os - \sigma ws} = 0.07$. For a water-wet system $\frac{\sigma_{ow}}{\sigma os - \sigma ws} \geq 1$. This implies that the geometrical roughness factor $\beta \approx 10^1 - 10^3$, consistent with literature roughness factor values defined by comparing surface areas measured with BET to those estimated by X-ray micro-CT imaging for other sandstone rocks (Lai et al., 2015). For additional information on model fitting and the choice of input parameters, please refer to the Support-

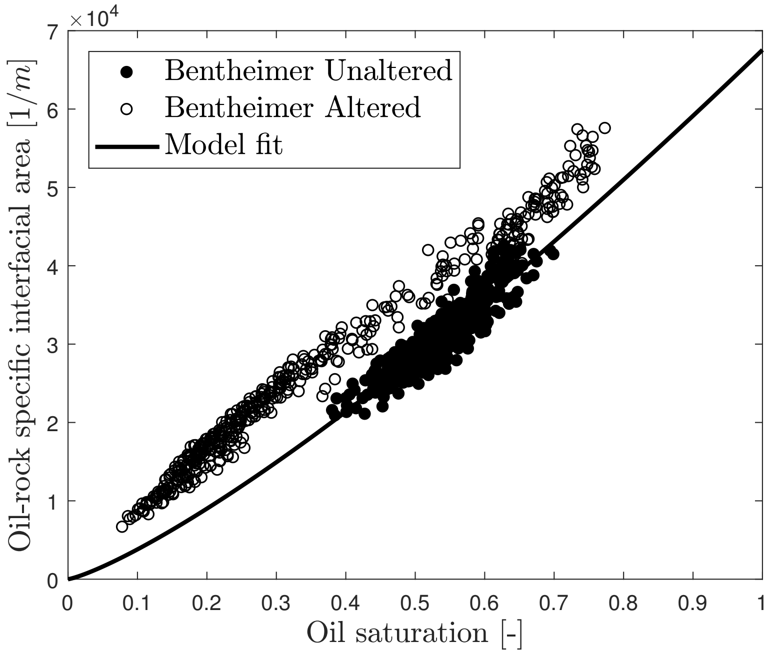

Figure 1. Oil-rock specific surface area measured in two Bentheimer sandstone datasets consisting of the X-ray micro-CT images of two steady-state imbibition experiments. For similar oil saturation values, the oil-coated specific surface areas are larger in the altered sample than in the unaltered one. The behaviour of the experimental data defined for Bentheimer Unaltered is reproduced by the model (Eq.2)

.

Table 1. Mineral volumetric composition and remaining fluid saturation (oil remaining saturation S_{or}, brine remaining saturation S_{wr}) after waterflooding from X-ray micro-CT images of the two Berea samples used in this study: Berea Unaltered (not aged by crude oil exposure) and Berea Altered (aged by crude oil exposure). The images were segmented in six phases: clay group minerals, quartz and feldspar, calcite cementation, other highly X-ray attenuating minerals, oil phase and brine phase.

	Berea Unaltered		Berea Altered	
	Mean [−]	St.Dev [−]	Mean [−]	St.Dev [−]
Clay	0.040	0.009	0.045	0.010
Quartz-Feldspar	0.840	0.046	0.813	0.043
Calcite	0.115	0.050	0.135	0.048
Others	0.006	0.004	0.006	0.004
S_{or}	0.572	0.050	0.239	0.071
S_{wr}	0.428	0.050	0.761	0.071

ing Information, where we also refer to Joekar-Niasar and Hassanizadeh (2012), Porter et al. (2009) and Raeesi et al. (2014).

Our methodology could be improved by the analysis of fluid coverage of rock surfaces on a pore-by-pore basis, in order to increase the level of detail in the topological description of wettability.

3.2 The role of rock surface mineralogy in controlling the wetting state

In this case the region of interest was divided as the previous case in cubic subvolumes of 300 voxels side, for a total of 64 subvolumes. In each of the subvolumes fluid saturations, mineral volume fractions and specific mineral fluid coating were computed.

3.2.1 Mineral composition and fluid saturation

The segmentation of the images of the two Berea sandstone samples led to similar mineral compositions (Table 1). This confirmed that the mineral segmentation workflow employed is reproducible. The largest component of the rock matrix is the quartz-feldspar group minerals. Cemented calcite constitutes the second most abundant mineral by volume fraction in the samples. Due to the process through which this cementation likely formed, it is pore filling, exposing mineral surfaces only to poorly accessible regions of the pore space. Segmented clay group minerals are broadly distributed, either as patches on quartz-feldspar or as clay aggregates.

The injection of 40 pore volumes of brine led to distinct values of remaining fluid saturation between the unaged and the aged samples. Berea Unaltered shows an average remaining oil saturation of 57%, while in Berea Altered oil displacement was more effective, leading to an average oil saturation of only 24%. Mixed-wet conditions are more favourable to the recovery of the oil phase as has been observed extensively on larger coreflood tests (Salathiel, 1973). As observed for the Bentheimer datasets, the variability in saturation is larger for the sample that underwent the wettability alteration procedure.

3.2.2 Fluid arrangement in the pore space

A visual inspection of the greyscale images acquired after waterflooding for the two samples clearly shows that the fluid arrangement differs. While in the unaltered sample, clay minerals are mainly filled with brine after the waterflooding, in the aged sample, brine is prevented from invading the small pores of the clay (Figure 2). This is a qualitative signal that ageing has affected clay preferential wetting to brine.

As shown for Bentheimer sandstone, we expect oil-coated surface area fraction to be positively correlated with oil saturation, i.e. the more oil in the pore space, the larger the fraction of mineral surface area contacted by oil. However, for both Berea Unaltered and Berea Altered this correlation is weak, as a consequence of the narrow range of fluid saturation in the experiment.

The oil-coated surface area fractions computed for Berea Unaltered suggest that all mineral groups considered are preferentially wetting to brine (Figure 3). Average oil-coated surfaces are always less than water coated surfaces even at high oil saturation. The average oil-coated clay surface area fraction is smaller than the quartz-feldspar fraction and this may be due to pore or fluid morphology, or sub-resolution roughness. The small pores found in these clays are preferentially imbibed by brine, due to the high capillary pressure required for the non-wetting phase to occupy them. Similarly, calcite cement mainly exposes its surface area to brine. This is a consequence of the capillary pressures associated with the narrow pore regions that the cementation did not clog when it formed. These findings are consistent with previous studies identifying these minerals as water-wet. In the unaged sample pore geometry and rock texture are likely to be responsible for the differences in the oil-coated mineral surface area fractions encountered. The system is uniformly water-wet.

In contrast, rock mineral heterogeneities do control wettability alteration during the ageing procedure. In Berea Altered, with a remaining oil saturation of 24%, 54% of clay surface area is coated by oil. This shows a strong change in the wetting preference of clay minerals, from water-wet to oil-wet. Even at lower oil saturation, there is much higher surface area coverage of clay minerals by oil in the altered sample relative to the unaltered sample. Similarly, a big increase is observed for cemented calcite, when results for Berea Unaltered are compared to those obtained for Berea Altered. On the other hand, quartz-feldspar does not show as strong of a wettability change. The reduced activity of quartz-feldspar surfaces during ageing compared to those of clay and calcite is consistent with what has been observed in Alipour Tabrizy et al. (2011), where clay and calcite surfaces have been found more prone to wettability alteration.

The specific mineral behaviours we have identified in the altered sample suggest that the wetting state is spatially correlated, with rock surface wetting preference changing with mineralogy. This may open up to the possibility of creating mixed wettability maps based on mineral topological characterisation.

4 Conclusions

The analysis of rock mineral surface coverage by fluids can depict differences in the wetting state of two fluid-phase systems. The solid surface covered by a fluid is positively correlated with the saturation of that fluid. The particular relationship between fluid saturation and fluid-mineral surface depends on the wetting state of the system. Considering the case of a uniformly water-wet system, we proposed a model that relates rock coverage to fluid saturation, fluid-fluid interfacial curvature and fluid-fluid interface extent, measurements easily acquired with X-ray micro-CT imagery. This model was validated by observations made before and after wetting alteration on a mineralogically homogeneous Bentheimer sandstone.

Rock surface coverage allowed us to investigate the role that mineralogy plays in defining the wetting state of two sandstone rocks. In an untreated rock sample with significant fractions of quartz, calcite, kaolinite and feldspar, fluid arrangement and surface coverage after a drainage and imbibition displacement sequence were consistent with a uniformly water-wet rock, regardless of local mineralogy. However, in a sample previ-

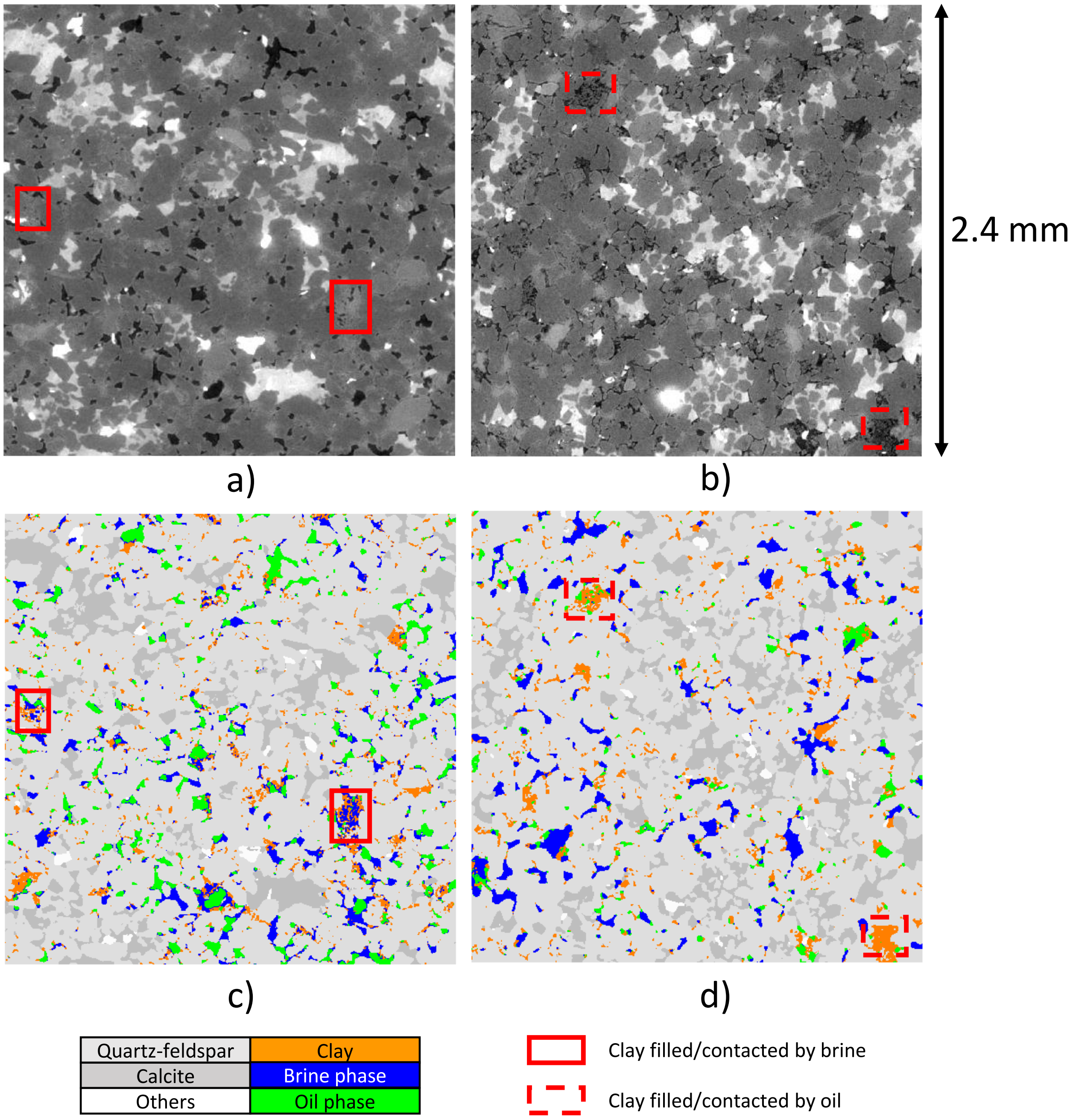

Figure 2. a) and b) show the greyscale images acquired after waterflooding of Berea Unaltered and Berea Altered, respectively. c) and d) show the segmented respective of a) and b). a) and b) show the change in clay wetting preference due to the effectiveness of the ageing protocol in Berea Unaltered and Berea Altered, respectively. In the sample Berea Unaltered clay aggregates are readily invaded by brine during waterflooding. In contrast, in the aged sample Berea Altered, brine invasion is largely prevented by the oil-wetting behaviour of clay surfaces.

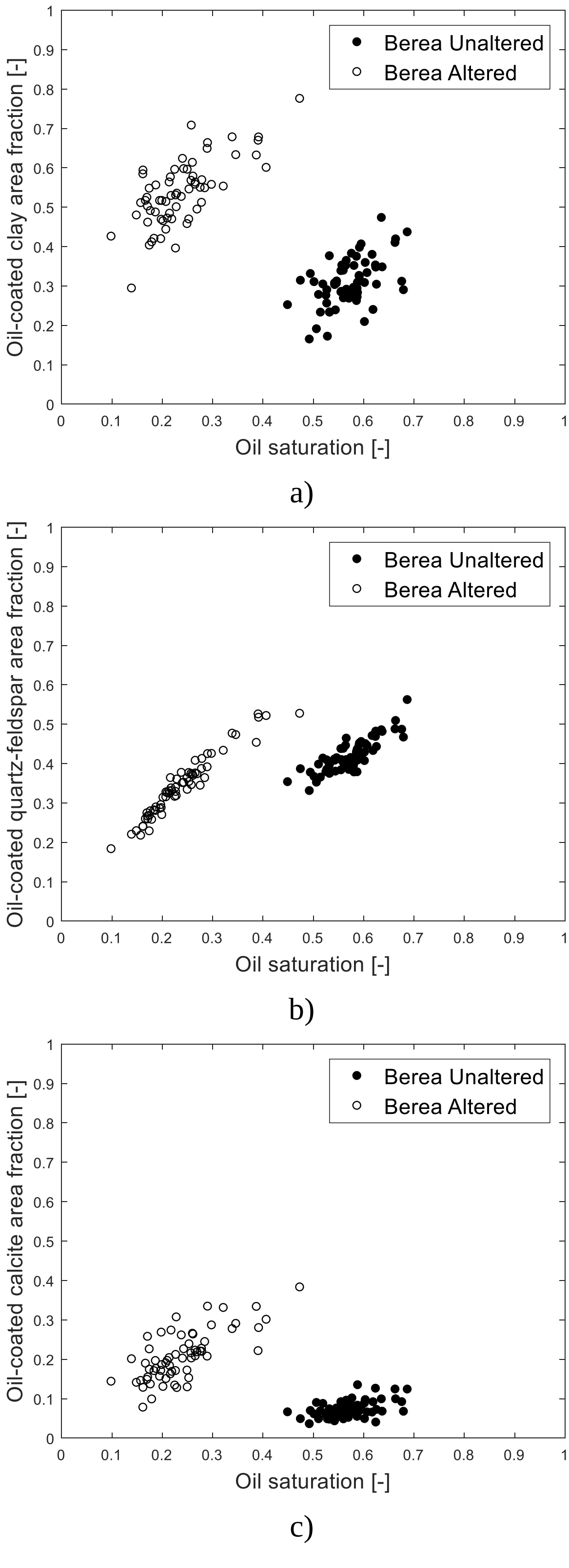

Figure 3. Oil-coated area fractions ($a_{i,j}$) computed in the two Berea sandstone samples imaged after waterflooding. Quartz-feldspar group minerals show similar coating in the two samples. Instead, clay and calcite minerals preferentially altered to an oil-wet state, with an average increase in the oil-coated area fraction of 74% and 184%, respectively.

ously exposed to crude oil and high temperature for 30 days, mineralogical heterogeneity has been found responsible for heterogeneous wettability alteration processes. Clay and calcite minerals were found more readily altered to an oil-wet state than quartz-feldspar minerals. As a consequence, the sample wetting state was heterogeneous, mixed-wet, with the distribution of the wetting state controlled by the local mineralogy.

Acknowledgments

We gratefully acknowledge Shell Global Solutions International B.V. for permission to publish this work. The Unaltered Bentheimer sandstone data are available from Lin, Bijeljic, Pini, et al. (2018b). The Altered Bentheimer sandstone dataset and Berea sandstone datasets will be available at Digital Rocks Portal (https://www.digitalrocksportal.org/, currently underway).

References

Alhammadi, A. M., AlRatrout, A., Singh, K., Bijeljic, B., & Blunt, M. J. (2017). In situ characterization of mixed-wettability in areservoir rock at subsurface conditions. *Scientific Reports*, *7*(1), 10753. Retrieved from `http://www.nature.com/articles/s41598-017-10992-w` doi: 10.1038/s41598-017-10992-w

Alipour Tabrizy, V., Denoyel, R., & Hamouda, A. A. (2011). Characterization of wettability alteration of calcite, quartz and kaolinite: Surface energy analysis. *Colloids and Surfaces A: Physicochemical and Engineering Aspects*, *384*(1-3), 98–108. Retrieved from `http://dx.doi.org/10.1016/j.colsurfa.2011.03.021` doi: 10.1016/j.colsurfa.2011.03.021

AlRatrout, A., Raeini, A. Q., Bijeljic, B., & Blunt, M. J. (2017). Automatic measurement of contact angle in pore-space images. *Advances in Water Resources*, *109*, 158–169. doi: 10.1016/j.advwatres.2017.07.018

Anderson, W. (1987a). Wettability Literature Survey- Part 4: Effects of Wettability on Capillary Pressure. *Journal of Petroleum Technology*, *39*(10), 1605–1622. doi: 10.2118/16471-PA

Anderson, W. (1987b). Wettability Literature Survey-Part 5: The Effects of Wettability on Relative Permeability. *Journal of Petroleum Technology*, *39*(12), 1605–1622. doi: 10.2118/16471-PA

Andrew, M., Bijeljic, B., & Blunt, M. J. (2014). Pore-scale contact angle measurements at reservoir conditions using X-ray microtomography. *Advances in Water Resources*, *68*, 24–31. Retrieved from `http://dx.doi.org/10.1016/j.advwatres.2014.02.014` doi: 10.1016/j.advwatres.2014.02.014

Berg, S., Ott, H., Klapp, S. A., Schwing, A., Neiteler, R., Brussee, N., … Others (2013). Real-time 3D imaging of Haines jumps in porous media flow. *Proceedings of the National Academy of Sciences*, *110*(10), 3755–3759. doi: 10.1073/pnas.1221373110

Beucher, S., & Meyer, F. (1993). The morphological approach to segmentation: the watershed transformation. *Mathematical Morphology in Image Processing*, 433–481. Retrieved from `https://www.crcpress.com/Mathematical-Morphology-in-Image-Processing/Dougherty/p/book/9780824787240` doi: ExportDate6May2013

Blunt, M. J., Jackson, M. D., Piri, M., & Valvatne, P. H. (2002). Detailed physics, predictive capabilities and macroscopic consequences for pore-network models of multiphase flow. *Advances in Water Resources*, *25*(8), 1069–1089.

Bradford, S. A., & Leij, F. J. (1997). Estimating interfacial areas for multi-fluid soil systems. *Journal of Contaminant Hydrology*, *27*(1), 83–105. Retrieved from `http://www.sciencedirect.com/science/article/pii/S0169772296000484` doi: https://doi.org/10.1016/S0169-7722(96)00048-4

Buades, A., Coll, B., Matem, D., Km, C. V., Mallorca, P. D., Morel, J.-m., & Cachan, E. N. S. (2005). A non-local algorithm for image denoising. (0), 0–5.

Buckley, J. S. (1998). Wetting Alteration of Solid Surfaces by Crude Oils and Their Asphaltenes. *Revue de l'Institut Français du Pétrole*, *53*(3), 303–312. doi: 10.2516/ogst:1998026

Buckley, J. S., & Liu, Y. (1998). Some mechanisms of crude oil/brine/solid interactions. *Petroleum Science and Engineering*, 155–160.

Buckley, S., & Leverett, M. (1942). Mechanism of fluid displacements in sands. *Transactions of the AIME*, *146*, 107–116.

Bultreys, T., Boone, M. A., Boone, M. N., De Schryver, T., Masschaele, B., Van Hoorebeke, L., & Cnudde, V. (2016). Fast laboratory-based micro-computed tomography for pore-scale research: Illustrative experiments and perspectives on the future. *Advances in Water Resources*, *95*, 341–351. Retrieved from http://dx.doi.org/10.1016/j.advwatres.2015.05.012 doi: 10.1016/j.advwatres.2015.05.012

Bultreys, T., De Boever, W., & Cnudde, V. (2016). Imaging and image-based fluid transport modeling at the pore scale in geological materials: A practical introduction to the current state-of-the-art. *Earth-Science Reviews*, *155*, 93–128. Retrieved from http://dx.doi.org/10.1016/j.earscirev.2016.02.001 doi: 10.1016/j.earscirev.2016.02.001

Coles, M. E., Hazlett, R., Muegge, E., Jones, K., Andrews, B., Dowd, B., ... W.E., S. (1996). Developments in synchrotron x-ray microtomography with applications to flow in porous media. *Society of Petroleum Engineers*, *1*(4), 288–296. doi: 10.2118/36531-MS

Donaldson, E. C., Thomas, R. D., & Lorenz, P. B. (1969). Wettability Determination and Its Effect on Recovery Efficiency. *SPE Journal*, 13–20. doi: 10.2118/2338-PA

Garfi, G., John, C. M., Berg, S., & Krevor, S. J. (2019). The sensitivity of estimates of multiphase fluid and solid properties of porous rocks to image processing. *EarthArXiv Preprints*. doi: 10.31223/osf.io/a23c7

Garing, C., de Chalendar, J. A., Voltolini, M., Ajo-Franklin, J. B., & Benson, S. M. (2017). Pore-scale capillary pressure analysis using multi-scale X-ray micromotography. *Advances in Water Resources*, *104*, 223–241. Retrieved from http://www.sciencedirect.com/science/article/pii/S0309170816305437 doi: https://doi.org/10.1016/j.advwatres.2017.04.006

Helgeson, H. C., Murphy, M., & Aagaard, P. E. R. (1984). Thermodynamic and kinetic constraints on reaction rates among minerals and aqueous solutions . II . Rate constants , effective surface area , and the hydrolysis of feldspar. , *48*(c), 2405–2432.

Herring, A. L., Middleton, J., Walsh, R., Kingston, A., & Sheppard, A. (2017). Flow rate impacts on capillary pressure and interface curvature of connected and disconnected fluid phases during multiphase flow in sandstone. *Advances in Water Resources*, *107*, 460–469. Retrieved from http://www.sciencedirect.com/science/article/pii/S0309170816307011 doi: https://doi.org/10.1016/j.advwatres.2017.05.011

Joekar-Niasar, V., & Hassanizadeh, S. M. (2012, sep). Uniqueness of Specific Interfacial Area–Capillary Pressure–Saturation Relationship Under Non-Equilibrium Conditions in Two-Phase Porous Media Flow. *Transport in Porous Media*, *94*(2), 465–486. Retrieved from https://doi.org/10.1007/s11242-012-9958-3 doi: 10.1007/s11242-012-9958-3

Klise, K. A., Moriarty, D., Yoon, H., & Karpyn, Z. (2016). Automated contact angle estimation for three-dimensional X-ray microtomography data. *Advances in Water Resources*, *95*. doi: 10.1016/j.advwatres.2015.11.006

Lai, P., Moulton, K., & Krevor, S. (2015). Pore-scale heterogeneity in the mineral distribution and reactive surface area of porous rocks. *Chemical Geology*, *411*(0), 260–273. Retrieved from http://linkinghub.elsevier.com/retrieve/pii/S0009254115003290 doi: 10.1016/j.chemgeo.2015.07.010

Lin, Q., Bijeljic, B., Berg, S., Pini, R., Blunt, M. J., & Krevor, S. (2019, Jun). Minimal surfaces in porous media: Pore-scale imaging of multiphase flow in an altered-wettability bentheimer sandstone. *Phys. Rev. E*, *99*, 063105. Retrieved from https://link.aps.org/doi/10.1103/PhysRevE.99.063105 doi: 10.1103/PhysRevE.99.063105

Lin, Q., Bijeljic, B., Krevor, S., Blunt, M., Berg, S., Coorn, A., ... Wilson, O. (2018). A new waterflood initialization protocol for pore-scale multiphase flow experiments. *International Symposium of the Society of Core Analysts,*, *SCA2018-03*, 1–12.

Lin, Q., Bijeljic, B., Pini, R., Blunt, M., & Krevor, S. (2018b). *Pore-scale imaging of multiphase flow at steady state for a bentheimer sandstone.* http://www.digitalrocksportal.org/projects/157. Digital Rocks Portal. doi: doi:10.17612/P7167R

Lin, Q., Bijeljic, B., Pini, R., Blunt, M. J., & Krevor, S. (2018a). Imaging and Measurement of Pore-Scale Interfacial Curvature to Determine Capillary Pressure Simultaneously With Relative Permeability. , 7046–7060. doi: 10.1029/2018WR023214

Morrow, N. R., & Szabo, J. O. (1970). Physics and Thermodynamics of Capillary. *Industrial and Engineering Chemistry*, *62*(6), 32–56. doi: 10.1021/ie50726a006

Porter, M. L., Schaap, M. G., & Wildenschild, D. (2009). Lattice-Boltzmann simulations of the capillary pressuresaturationinterfacial area relationship for porous media. *Advances in Water Resources*, *32*(11), 1632–1640. Retrieved from http://www.sciencedirect.com/science/article/pii/S0309170809001328 doi: 10.1016/j.advwatres.2009.08.009

Raeesi, B., Morrow, N., & Mason, G. (2014). Capillary pressure hysteresis behaviour of three sandstones measured with a multistep outflow-inflow apparatus. *Vadose Zone Journal*, *13*(3). doi: 10.2136/vzj2013.06.0097

Rücker, M., Bartels, W. B., Singh, K., Brussee, N., Coorn, A., van der Linde, H. A., ... Berg, S. (2019). The Effect of Mixed Wettability on Pore-Scale Flow Regimes Based on a Flooding Experiment in Ketton Limestone. *Geophysical Research Letters*, *46*(6), 3225–3234. doi: 10.1029/2018GL081784

Salathiel, R. (1973). Oil recovery by surface film drainage in mixed-wettability rocks. *Petroleum Technology*, *25*, 1216–1224. doi: 10.2118/4104-PA

Scanziani, A., Singh, K., Blunt, M. J., & Guadagnini, A. (2017). Automatic method for estimation of in situ effective contact angle from X-ray micro tomography images of two-phase flow in porous media. *Journal of Colloid and Interface Science*, *496*, 51–59. Retrieved from http://dx.doi.org/10.1016/j.jcis.2017.02.005 doi: 10.1016/j.jcis.2017.02.005

Singh, K., Bijeljic, B., & Blunt, M. (2016). Imaging of oil layers, curvature, and contact angle in a mixed-wet and a water-wet carbonate rock. *Water Resource Research*, *52*, 1716–1728. doi: 10.1002/2015WR018072

White, A. F., & Peterson, M. L. (1990). Role of Reactive-Surface-Area Characterization in Geochemical Kinetic Models.

Zou, S., Armstrong, R. T., Arns, J.-Y., Arns, C., & Hussain, F. (2018). Experimental and Theoretical Evidence for Increased Ganglion Dynamics During Fractional Flow in Mixed-Wet Porous Media. *Water Resources Research*, 3277–3289. doi: 10.1029/2017WR022433